TIERS Information Technology Journal
Vol.4, No.2, December 2023, pp. 92~103
ISSN: 2723-4533 / E-ISSN: 2723-4541
DOI: 10.38043/tiers.v4i2.4468

Java and Bali Shoreline Change Detection Based on Structural Similarity Index Measurement of Multispectral Images

I Gede Wahyu Surya Dharma[1], I Gede Karang Komala Putra[2]
suryadharma@iikmpbali.ac.id[1], igdkarang@iikmpbali.ac.id[2]
Faculties of Business, Social, Technology and Humanities, Universitas Bali Internasional, Denpasar

ABSTRACT

The abstract effectively delineates the pertinent issues addressed in the research, presenting a clear exposition of the challenges associated with coastline monitoring in Indonesia. The methodology is well-defined, incorporating the utilization of Landsat images, Structural Similarity Index Measurement (SSIM), and the application of Hidden Markov Random Field for segmentation. Moreover, the influence of Indonesia's equatorial positioning on cloud cover and the subsequent application of morphological operations are appropriately highlighted. However, it is crucial to provide explicit details regarding the research findings. Specifically, the abstract should elucidate the specific outcomes or results obtained from the conducted experiments or analyses. This addition would enhance the clarity and scientific robustness of the abstract, ensuring that it accurately reflects the research objectives and their corresponding achievements. Inclusion of quantitative data or statistical analyses would be particularly valuable in this regard. This would not only bolster the abstract but also furnish a more comprehensive overview of the study's empirical contributions.

Keywords: SSIM; HMRF; Shoreline; Multispectral Image

Article Info

Accepted : 10-12-2023
Revised : 09-09-2023
Published Online : 23-12-2023

Correspondence Author:

I Gede Wahyu Surya Dharma,
Informatics Engineering Study,
Faculties of Business, Social, Technology and Humanities, Universitas Bali Internasional, Denpasar, Indonesia
Email: suryadharma@iikmpbali.ac.id

1. INTRODUCTION

Every year, numerous tourists visit Indonesia, drawn by the allure of its beaches and natural beauty. Particularly in Bali and the Javanese areas, renowned for their exceptionally beautiful beaches, there arises the necessity for continuous supervision and monitoring of the shape and extent of the existing coastlines. The perils posed by tsunamis, coastal erosion, and rising sea levels present a grave threat to the residents and workers inhabiting these coastal regions [1]. The coastline, a pivotal demarcation between the marine and terrestrial realms [2], serves as an indicator of the recent implications of global warming. Moreover, the equatorial locale of Indonesia gives rise to distinctive natural conditions, characterized by the dense cloud cover that blankets most of the nation's territories. This

poses a challenge for researchers engaged in change detection and remote sensing within coastal zones, as they must contend with the substantial cloud cover. Notably, shoreline observations hold immense significance due to their ever-evolving nature over time.

Prior investigations have predominantly centered on the cartography of coastal areas to preclude and identify potential disasters, facilitating the implementation of appropriate mitigation strategies. Areas densely populated along the coastline[1] confront the dilemma of abrupt surges in sea levels, which could inundate their habitation. Consequently, early detection becomes pivotal in averting major disasters, thereby allowing residents to evacuate promptly [2].

However, conducting comprehensive analyses primarily employing multispectral imagery and remote sensing methodologies introduces a formidable challenge—namely, the voluminous data combined with the prevailing simplicity of processing techniques. Furthermore, the scarcity of computational resources and expertise further compounds this challenge [1]. This, in turn, translates into prolonged analysis durations for multispectral imagery.

The structural similarity index measurement method, known as SSIM, emerges as a prudent choice for conducting change detection analyses. In a study conducted by Yavariabdi et al., the SSIM method was employed to scrutinize Landsat images, enabling the quantification of significant changes by comparing reference images with those affected by the presence of fog and thin cloud cover [3]. This approach can be effectively transposed to the present study, accommodating the cloud-covered areas observed in Indonesia. However, due to the notably widespread cloud cover across Indonesia, an alternative approach is requisite to surmount this obstacle.

In the present study, the structural similarity index measurement method is employed to discern substantial alterations in the coastal regions of east Java and west Bali spanning the years from 2013 to 2017. Furthermore, a hidden Markov random field is employed to differentiate between sea and land segments, following the removal of cloud interference through pre-processing and morphological operations. The integration of these pre-processing and morphological operations aims to bolster the quality and accuracy of similarity measurements by eliminating noise arising from cloud formations.

2. RESEARCH METHOD

Focusing on this research are the shorelines of West Bali and East Java Island. This location was chosen due to the rapid development of Bali and East Java since the year 2000. Many people relocate to Bali for residency, work, or vacation, and when people visit Bali or Java, it is often to enjoy the beaches. Monitoring the beach areas or shorelines allows for quicker disaster or erosion detection, enabling prompt and effective response.

Figure 1. Study Area

Multispectral images from the Landsat official website of the National Institute of Aeronautics and Space (LAPAN) Indonesia are utilized as the dataset for this research. The images procured from LAPAN are concentrated on the shorelines of East Java and West Bali. The images employed in this study are captured by satellites using

Landsat 5 and 8, featuring three levels of correction: L1G, L1T, and L1GT [4]. To acquire these images, the initial step involves selecting the coastal area using a bounding box to extract more specific information associated with these images. Subsequently, a time series of data spanning from 2013 to 2017 is chosen within the same location, ensuring the research is directed toward particular and predefined areas.

As demonstrated in Figure 2 below, examples of Landsat 5 and Landsat 8 images obtained from the LAPAN catalog are provided.

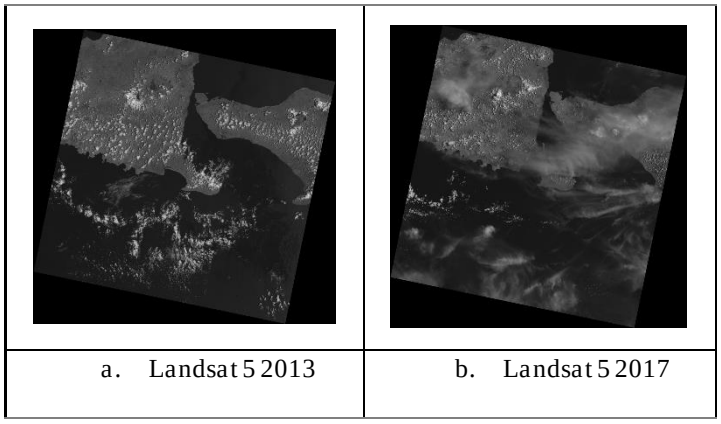

a. Landsat 5 2013 b. Landsat 5 2017

Figure 2. Landsat Multi temporal Images

This study uses multispectral Landsat images to analyze the land cover changes in Indonesia. However, these images may have some limitations, such as spatial or spectral noise, which can affect the accuracy and quality of the analysis. Spatial noise refers to random variations in pixel values that are not related to the actual features of the image, while spectral noise refers to variations in the spectral signatures of the same land cover type. These noises can be caused by various factors, such as atmospheric conditions, sensor errors, or human errors. Moreover, Indonesia is located near the equator, which means that it often has a high percentage of cloud cover throughout the year [5]. Clouds can obscure the underlying land surface and introduce errors in the classification of land cover types [6].

To address these challenges, this study applies some additional methods to improve the quality of the Landsat images before performing the land cover change analysis. These methods include pre-processing and morphological operations. Pre-processing is a general term that refers to various techniques that can enhance the contrast, reduce the noise, or correct the geometric distortions of an image [7]. Some examples of pre-processing techniques are radiometric correction, atmospheric correction, histogram equalization, filtering, and resampling [8]. Morphological operations are a specific type of image processing techniques that can modify the shapes and structures of the image based on a predefined structuring element. Some examples of morphological operations are erosion, dilation, opening, closing, and gradient. These operations can be used to remove unwanted objects, such as clouds and shadows, from the image, or to fill in the gaps or holes in the image [7].

This study not only applies these methods to the Landsat images, but also compares the results of the land cover change analysis between the pre-processed and non-pre-processed images. The purpose of this comparison is to evaluate the effectiveness and impact of these methods on the accuracy and quality of the land cover change analysis. By doing so, this study aims to provide a better understanding of the land cover dynamics in Indonesia and the challenges and solutions of using Landsat images for this purpose.

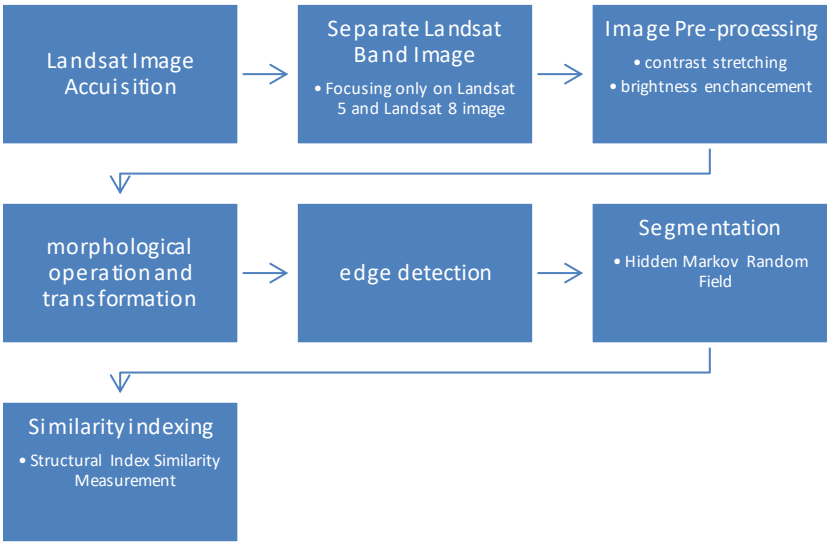

Figure 3. Research stages

The Landsat images captured in Indonesia often confront cloud cover, rendering analysis using optical images a slightly challenging endeavor. The conventional approach to rectify such issues involves applying pre-processing phases. In image processing, pre-processing comprises a series of operations designed to enhance image quality by mitigating geometrical distortions, noise, or initial image quality issues. Techniques like contrast stretching, brightness enhancement, edge detection, morphological operations, and transformation are executed to mitigate noise from the images.

The Landsat images, presented in grayscale, exhibit slight similarity in pixel values between sea, shoreline, and land areas. Conversely, clouds manifest significantly distinct pixel values. However, some land or sea areas may also exhibit similar pixel values to clouds due to sunlight reflection. This presents a challenging scenario, as it can influence the classification of shoreline areas, where cloud-induced noise could lead to misclassifications.

The integration of pre-processing and morphological operations occurs within a single phase. Initially, each image is resized, divided into 30 specific areas in West Bali and East Java.

Pre-processing and Morphological Operations

As previously discussed, the prevalence of cloud cover across Indonesia necessitates an auxiliary approach to eliminate clouds and enhance image clarity, particularly for shoreline regions. Therefore, the morphological operation is chosen due to its capacity to eliminate unwanted edges or regions. To effect cloud removal, image adjustment is first applied to calibrate image intensity values or color maps. This adjustment aims to enhance contrast for clearer differentiation between sea, land areas, and clouds. The application of a median filter, a nonlinear operation, serves to mitigate "salt and pepper" noise [9]. In this study, the median filter is employed to reduce the presence of small noise regions and enhance system robustness. Morphological operations such as erosion and filling, implemented in this study, necessitate images to be in a binary or black-and-white format. Erosion, employing a 5x5 diamond-shaped structuring element, is performed multiple times within specific image areas [10].

Edge detection and Gaussian filtering

As depicted in the flowchart, edge detection and Gaussian filtering are executed as distinct phases. The process of gray-scaling is omitted, given that Landsat images are already in grayscale format. This is followed by edge detection, aimed at identifying pixel intensity shifts occurring sharply within a brief period [11]. Edge detection serves to segment an area into two distinct regions. The edges themselves are distinctly visualized, bearing directional attributes that determine adjacency and orientation. The determination of adjacency and orientation is predicated on changes in pixel intensity values. Notably, three types of edges are recognized [12]:

1. Steep Edges: Characterized by a significant change in pixel value intensity.
2. Sloping Edges: These edges encompass a broader spatial extent and possess a relatively smaller directional angle. They consist of edges that are locally adjacent.
3. Noising Edges: These edges not only carry pixel value information but are also accompanied by noise that compromises image quality. The noise pixel values within the image exhibit significant changes between noise values and background image values [13].

Hidden Markov random field – Landsat image segmentation

Given a random field X where X is a finite lattice of set I on the neighborhood system in a set of random variables. Where X is denoted by $X = \{Xi \,|i \in I\}$. There are two condition that need to be established to denote X as the neighborhood system Markov random field:

$p(x) > 0$

$p(x_i|x_{i-\{i\}}) = p(x_i|x_{\partial i})$

Hidden Markov random field model denoted by X, Y where X, Y is a coordinate point of two-dimensional lattice where I is a set of random fields. Respectively, corresponding value denoted with $\Psi_x = \{1, \dots, L\}$ and $\Psi_y = \{1, \dots, M\}$. Joint event of X denoted as $X_1 = x_1, \dots, X_N = x_N$ where $X = \{Xi \,|i \in I\}$. Joint event of Y denoted as $Y_1 = y_1, \dots, Y_M = y_M$ where $Y = \{Yi \,|i \in I\}$. Probability of each occurrence $X_i = x_i$ is denoted by $p(X_i = x_i)$ symbolized as $p(x_i)$. Probability of each occurrence $Y_i = y_i$ is denoted by $p(Y_i = y_i)$ symbolize as $p(y_i)$. Markov random field denoted as X that satisfy Markov property where $p(x) > 0$ and $p(x_i|x_{i-\{i\}}) = p(x_i|x_{\partial i})$ [14]. Hidden Markov random field which defined as (X, Y) in random process denoted by

$$p(x) = \prod_{i \epsilon S} p(y_i|x_i) \quad (1)$$

Known that X is the Markov random field where the random process is unobserved, Y represents an observed random process. Notably, hidden Markov random field satisfy that (X,Y) has Markov properties and joint distribution of hidden Markov random field (X,Y) [15]is

$$p(y, x) = p(x)p(x)$$
$$p(x) = \prod_{i \epsilon S} p(x_i) \quad (2)$$

Structural similarity index measurement – Landsat image similarity measurement

In this study, change detection measurement is carried out by utilizing the structural similarity index measurement (SSIM). For similarity measurement, two distinct Landsat images are chosen. Typically, when comparing two different images, the method of choice is image subtraction [16]. However, due to the unique characteristics of Landsat images, image subtraction proves to be less reliable in accounting for changes in contrast, brightness, and color differences [17]. Consequently, the SSIM approach is adopted for change detection measurement, as it is adept at identifying variations in intensity *s*, brightness *l*, and contrast *c* between the two Landsat images. The calculation of SSIM [18]is as follows:

$$X_d^{(n)} = [l(X_1^{(n)}, X_2^{(n)})]^{\alpha}[c(X_1^{(n)}, X_2^{(n)})]^{\beta}[s(X_1^{(n)}, X_2^{(n)})]^{\gamma} \quad (3)$$

Where α, β, and γ are the exponents, where the final calculation of X_d is using these three parameters to adjust the influence of each measurement. Where α = β = γ = 1, the variable l, c, s can be written as:

$$\{l(X_1^{(n)}, X_2^{(n)}) = \frac{2\mu_{X_1^{(n)}}\mu_{X_2^{(n)}}}{\mu_{X_1^{(n)}} + \mu_{X_2^{(n)}} + \epsilon 1}\; c(X_1^{(n)}, X_2^{(n)}) = \frac{2\sigma_{X_1^{(n)}}\sigma_{X_2^{(n)}}}{\sigma_{X_1^{(n)}} + \sigma_{X_2^{(n)}} + \epsilon 2}\; s(X_1^{(n)}, X_2^{(n)}) = \frac{\sigma_{X_1^{(n)}}\sigma_{X_2^{(n)}}}{\sigma_{X_1^{(n)}} + \sigma_{X_2^{(n)}} + \epsilon 3}$$

As shown above, σ, μ and σX_1X_2 respectively are mean, standard deviation, and covariance between two images, and also ε_1, ε_2, ε_3 are small positive constants. These positive constants aim to avoid instability.

3. RESULTS AND DISCUSSION

Image Acquisition

The sequence of the image acquisition process begins with the selection and download of images from the Java and Bali shorelines, designated as regions of interest, via the Landsat catalog of LAPAN: http://landsat-catalog.lapan.go.id/. These shorelines are situated in East Java and West Bali, spanning from the year 2013 to 2017.

The images procured for this study comprise approximately 6 images captured in Band 5 during the years 2013, 2014, and 2017. Specifically, one image from August 28th, 2013, is designated as the ground truth, followed by 3 images from June 7th, 2014, September 3rd, 2014, and December 5th, 2014, respectively. Additionally, 2 images from March 5th, 2017, and May 9th, 2017, are included in the dataset for the year 2017. To streamline processing time, each image is subdivided into 19 images of comparable size and resolution, enhancing processing efficiency. Figure 4 provides an illustration of the East Java and West Bali region utilized in this study [19].

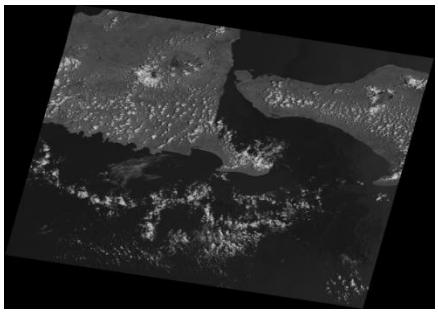

Figure 4. *Selected image of Java and Bali*

Each image possesses an approximate resolution of 7491x7291 pixels. Given that this resolution is not in a standard format, a resolution adjustment is implemented, resizing each image to 7490x7290 pixels to meet the desired criteria. The substantial resolution of Landsat images can result in prolonged processing times and hinder the analysis of differences between two such images. To address this concern, the initial resolution is subdivided into 19 smaller images, each concentrating on a specific area for analysis [20]. These 19 smaller Landsat images pertain to distinct areas within the East Java and West Bali regions, encompassing both smaller and larger areas affected by cloud coverage. Figure 5 offers a visual comparison between the default resolution and the half-resolution of Landsat images from 2013 (ground truth) and 2017 (comparison images).

Image Preprocessing - Morphological Operation

Landsat images exhibit relatively large resolutions, capturing expansive Earth regions through optical sensors mounted on satellites. These images, known as multispectral images, encompass numerous bands, exceeding 5 bands, each delineating distinct geographic characteristics within the area. Although individual bands adhere to grayscale color maps, they collectively yield colorful composite images that vividly portray the area's geographic traits and conditions. This results in Landsat images featuring resolutions surpassing 7000x7000 pixels. Consequently, to address protracted processing times and excessive memory utilization, as previously elucidated, Landsat images are partitioned into 19 smaller images, each boasting a resolution of 962x962 pixels. This resolution choice ensures expedited processing and minimizes memory requirements.

Due to the grayscale nature of the image color maps, a contrast limit ranging from 0.1 to 0.3 is assigned to each pixel within each image. This is aimed at enhancing contrast with a higher intensity threshold set at 0.3. Following the image enhancement stage, the subsequent step involves applying a median filter to eradicate minor cloud noise. A diamond-shaped structural element is employed for erosion application, particularly targeting undesirable elements, notably clouds that manifest within the images. Lastly, a process of image filling is executed to address any remaining gaps or indistinct areas, ensuring comprehensive determination of all regions.

The application of image pre-processing and morphological operations proves crucial for cloud noise removal, given the pervasive cloud coverage across East Java and West Bali. This cloud interference profoundly

influences the outcomes of image comparisons, as differing cloud densities could yield inaccurate results in terms of comparative measurements. The visual contrast between the original and enhanced images is presented in Figure 5.

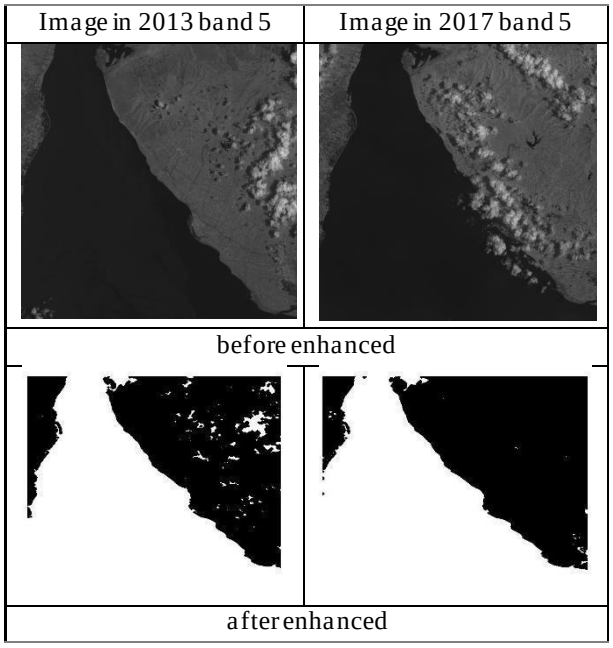

Figure 5. Images before and after enhanced

Hidden Markov Random Field – Image Segmentation

If image pre-processing and morphological operations are employed as input for similarity measurement using the structural index, the resulting output may indicate a more extensive altered area. However, this could be misleading, as we are aware that the actual alterations are minimal and primarily attributed to cloud cover. Consequently, an image segmentation methodology is deemed essential to achieve a precise demarcation of regions encompassing land, sea, shoreline, and cloud [21].

Hidden Markov Random Fields (HMRFs) have proven to be a potent tool in the domain of hyperspectral image segmentation. A hyperspectral image is characterized by a high-dimensional feature space, encompassing spectral information across numerous contiguous narrow bands. The segmentation task entails delineating distinct regions within the image, each corresponding to unique materials or entities, through an integrated consideration of both spectral and spatial cues.

Within the HMRF framework, the hyperspectral image is represented as a graph, where nodes correspond to pixels and edges model the spatial relationships between them. The latent variables, constituting the 'hidden' aspect of the model, represent the class labels associated with each pixel. These latent states are inferred via an amalgamation of observed spectral signatures and contextual spatial dependencies.

Mathematically, the energy function E governing the HMRF model can be formulated as:

$$E(X,Y) = \sum_i U(x_i,y_i) + \sum_{(i,j)} V(x_i,x_j,y_i,y_j)$$

Here, X denotes the set of latent variables (class labels), Y represents the observed hyperspectral data, x_i and y_i are the latent and observed values respectively for pixel i, and U and V denote the unary and pairwise potentials, respectively.

1. **Unary Potentials (U):** This term encapsulates the compatibility between observed spectral features and assigned class labels. It is expressed as:
$$U(x_i,y_i) = -\log P(y_i|x_i)$$
where $P(y_i|x_i)$ denotes the likelihood of observing spectral signature y_i given class label x_i.

2. **Pairwise Potentials (V):** These potentials encode the contextual relationships between adjacent pixels, encouraging spatial coherence in the segmentation. They are defined as:

$$V(x_i, x_j, y_i, y_j) = \lambda_{ij} \cdot \Pi(x_i \neq x_j) \cdot \phi(y_i, y_j)$$

Here, λ_{ij} represents the spatial coupling strength between pixels i and j, $\Pi(x_i \neq x_j)$ is the indicator function, and $\phi(y_i, y_j)$ models the compatibility of spectral signatures.

The objective is to determine the labeling configuration that minimizes the energy function, a task often accomplished through optimization techniques such as the Expectation-Maximization (EM) algorithm or graph cuts.

Equation for Post-Processing the Segmented Binary Image:

Post-processing steps, critical for refining segmentation outcomes, often involve morphological operations. Specifically, to eliminate small incongruent regions and noise, the following operations can be employed:

1. **Erosion:**

$I_{\text{eroded}} = I \ominus B$

Here, I represents the binary image, B is the structuring element, and $\ominus$ denotes erosion.

2. **Dilation:**

$I_{\text{dilated}} = I_{\text{eroded}} \oplus B$

This operation restores the size of larger regions and ensures spatial coherence.

The Hidden Markov random field serves as an image segmentation technique that preserves edge information and efficiently segments 2D images by eliminating undesired small areas. To expunge these extraneous elements within the images, images subjected to pre-processing, images processed with Gaussian filters, and edge images are collectively input into the Hidden Markov random field framework. Figure 6 visually depicts the outcome of applying the Hidden Markov random field, yielding a substantially clearer representation of areas with reduced cloud interference

In summary, the judicious application of HMRFs in conjunction with morphological operations facilitates robust hyperspectral image segmentation by harnessing both spectral and spatial information.

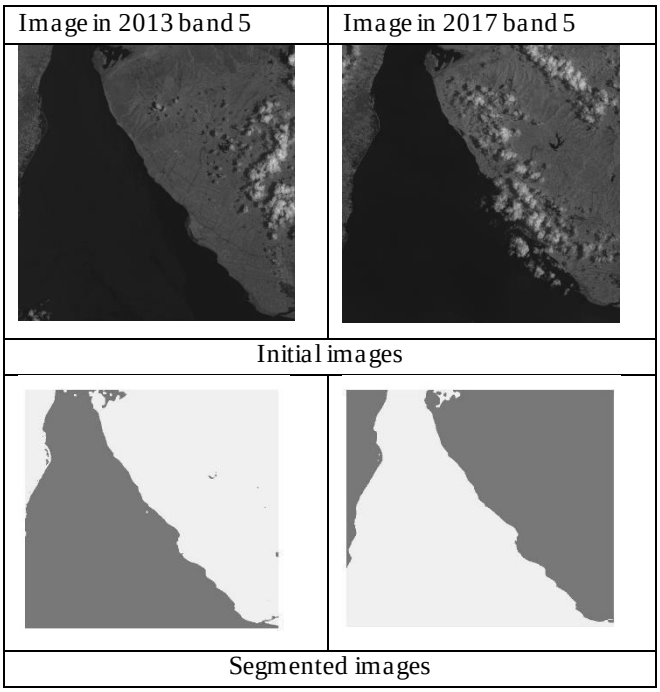

Figure 6. Images before and after segmented

Structural Similarity Index Measurement

For the purpose of comparing two binary or RGB images, image subtraction is commonly employed to gauge the percentage or discrepancies between these images. However, due to the inherent susceptibilities of Landsat images to variations in contrast, brightness, and color differences, traditional image subtraction is not robust. Consequently, the adoption of the structural similarity index measurement (SSIM) is chosen to discern the likeness between two images across contrast, brightness, and color disparities [17]. The SSIM method contrasts with frequently used similarity metrics like image differencing or log ratios, as it assesses image differences in terms of structural information alterations.

The application of the SSIM method involves comparing the ground truth and comparing Landsat images, which have been previously subdivided and segmented prior to undergoing pre-processing and Hidden Markov random field techniques. These images, possessing dimensions of 962x962 pixels, facilitate a more targeted similarity assessment, as each image is compared with its corresponding counterpart. This approach offers a simplified analytical process, compared to utilizing raw images where identifying areas of significant change could prove challenging.

Figure 7 illustrates the comparison between the ground truth image from the year 2013 and the comparison images from the years 2014 and 2017.

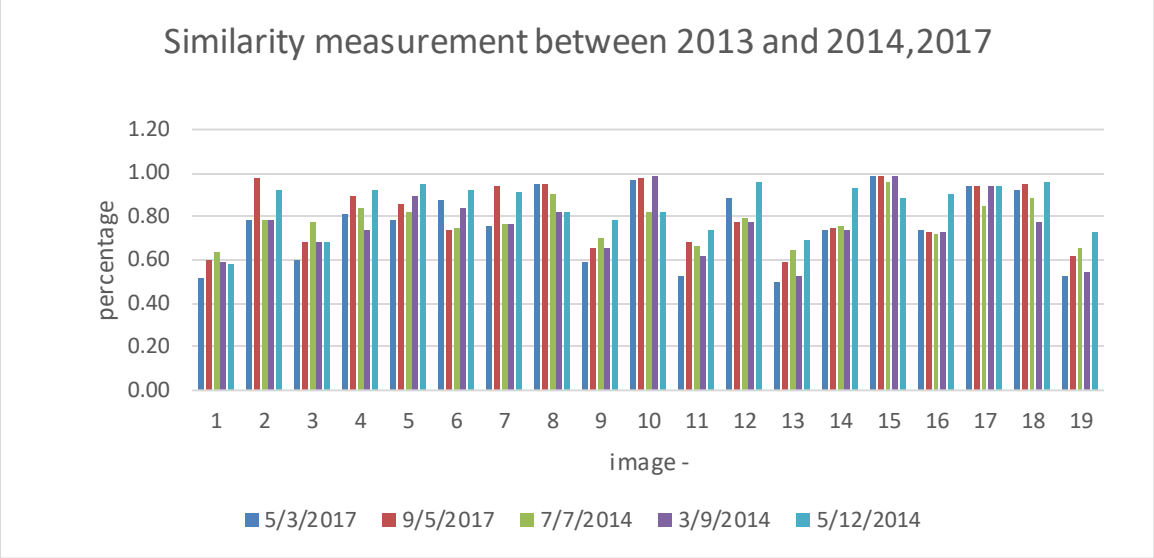

Figure 7. Result of similarity measurement

Figure 7 presents the outcomes of the similarity measurement conducted between the years 2013 and 2014, as well as 2017. The provided values reveal that specific areas exhibit similarity indices lower than 0.8, suggesting alterations exceeding 20% compared to the ground truth images. Notably, certain regions demonstrate similarity indices in the range of 0.5 to 0.6, signifying an approximate 40% change. However, it is noteworthy that some areas register values close to 1, implying an exact correspondence to the ground truth.

Nonetheless, upon inspecting Table 1, which offers a concise summary of the outcomes, more nuanced insights emerge. For instance, image number 2 from May 9th, 2017, attains a similarity index of 0.98, while the image from December 5th, 2014, records a similarity index of 0.92. Conversely, other dates yield a similarity index of approximately 0.78. This discrepancy could suggest that dates achieving a similarity index of 0.78 are marred by dense clouds, requiring additional methodologies for effective cloud removal. The proposed approach may prove insufficient for eliminating such dense clouds. Clouds pose a challenge to shoreline change detection due to the sensitivity of pixel values between sea and land areas to cloud interference. When clouds appear in the shoreline region, they can distort shoreline length detection and yield erroneous recognition of altered shoreline areas.

The outcomes derived from the SSIM method are significantly influenced by preceding processes, including image segmentation, pre-processing, and image enhancement, which collectively enhance the quality of Landsat images. Therefore, it becomes evident that a more comprehensive approach is requisite to yield representative measurement outcomes. This entails incorporating cloud removal methodologies that account for a broader array of scenarios. For instance, under conditions featuring thin and fog-like clouds, the application of additional morphological operations becomes unnecessary, as the optical sensors can effectively capture the observed region.

Table 1. Result of similarity measurement between ground truth in year of 2013 and comparison images in 2014 and 2017.

	5/3/2017	**9/5/2017**	**7/7/2014**	**3/9/2014**	**5/12/2014**
1	0.52	0.60	0.64	0.59	0.58
2	0.78	0.98	0.79	0.79	0.92
3	0.60	0.68	0.78	0.68	0.68
4	0.81	0.89	0.84	0.74	0.92
5	0.78	0.86	0.82	0.90	0.95
6	0.87	0.74	0.75	0.84	0.92
7	0.75	0.94	0.77	0.77	0.92

8	0.95	0.95	0.90	0.82	0.82
9	0.59	0.66	0.70	0.66	0.78
10	0.97	0.98	0.82	0.99	0.82
11	0.53	0.68	0.66	0.62	0.74
12	0.89	0.77	0.79	0.77	0.96
13	0.50	0.59	0.65	0.52	0.69
14	0.74	0.74	0.75	0.74	0.93
15	0.99	0.99	0.96	0.99	0.89
16	0.74	0.73	0.72	0.73	0.90
17	0.94	0.94	0.84	0.94	0.94
18	0.92	0.95	0.88	0.78	0.96
19	0.53	0.61	0.66	0.54	0.73

4. CONCLUSION

The conclusion provided in the manuscript appropriately discusses the effectiveness of the Hidden Markov random field methodology for achieving accurate segmentation outcomes, particularly in delineating sea and land regions. The impact of this successful segmentation on similarity measurement results is duly noted. Lower similarity values are suggested to potentially signify areas heavily affected by dense cloud formations, a phenomenon attributed to Indonesia's equatorial positioning. Additionally, the integration of morphological operations is emphasized as a necessary step in mitigating cloud-induced noise.

However, to align the conclusion with the research objectives, it is advised to incorporate specific research findings. This would further enhance the clarity and scientific rigor of the conclusion, ensuring that it directly addresses the research goals and outcomes. The inclusion of quantitative results or statistical analyses pertaining to the segmentation accuracy and its relationship with cloud cover would be particularly beneficial. This would not only bolster the conclusion but also provide a more comprehensive summary of the study's findings.

REFERENCES

[1] M. A. Marfai, H. Almohammad, S. Dey, B. Susanto, and L. King, "Coastal dynamic and shoreline mapping: multi-sources spatial data analysis in Semarang Indonesia," *Environ. Monit. Assess.*, vol. 142, no. 1–3, pp. 297–308, Jul. 2008, doi: 10.1007/s10661-007-9929-2.

[2] Y. Wang, X. Hou, P. Shi, and L. Yu, "Detecting Shoreline Changes in Typical Coastal Wetlands of Bohai Rim in North China," *Wetlands*, vol. 33, no. 4, pp. 617–629, Aug. 2013, doi: 10.1007/s13157-013-0418-9.

[3] A. Yavariabdi and H. Kusetogullari, "Change Detection in Multispectral Landsat Images Using Multiobjective Evolutionary Algorithm," *IEEE Geosci. Remote Sens. Lett.*, vol. 14, no. 3, pp. 414–418, Mar. 2017, doi: 10.1109/LGRS.2016.2645742.

[4] H. Othman and S. E. Qian, "Noise reduction of hyperspectral imagery using hybrid spatial-spectral derivative-domain wavelet shrinkage," *IEEE Trans. Geosci. Remote Sens.*, vol. 44, no. 2, pp. 397–408, 2006, doi: 10.1109/TGRS.2005.860982.

[5] D. S. Candra, S. Phinn, and P. Scarth, "Cloud and cloud shadow removal of landsat 8 images using Multitemporal Cloud Removal method," in *2017 6th International Conference on Agro-Geoinformatics*, IEEE, Aug. 2017, pp. 1–5. doi: 10.1109/Agro-Geoinformatics.2017.8047007.

[6] R. Cao, Y. Chen, J. Chen, X. Zhu, and M. Shen, "Thick cloud removal in Landsat images based on autoregression of Landsat time-series data," *Remote Sens. Environ.*, vol. 249, p. 112001, Nov. 2020, doi: 10.1016/j.rse.2020.112001.

[7] Y. Chen, Q. Weng, L. Tang, X. Zhang, M. Bilal, and Q. Li, "Thick Clouds Removing From Multitemporal Landsat Images Using Spatiotemporal Neural Networks," *IEEE Trans. Geosci. Remote Sens.*, vol. 60, pp. 1–14, 2022, doi: 10.1109/TGRS.2020.3043980.

[8] S. Bostan, M. A. Ortak, C. Tuna, A. Akoguz, E. Sertel, and B. Berk Ustundag, "Comparison of classification accuracy of co-located hyperspectral & multispectral images for agricultural purposes," *2016 5th International*

Conference on Agro-Geoinformatics, Agro-Geoinformatics 2016. 2016. doi: 10.1109/Agro-Geoinformatics.2016.7577671.
[9] F. Wu, X. Y. Jing, X. You, D. Yue, R. Hu, and J. Y. Yang, "Multi-view low-rank dictionary learning for image classification," *Pattern Recognit.*, vol. 50, pp. 143–154, 2016, doi: 10.1016/j.patcog.2015.08.012.
[10] S. Li, T. Lu, L. Fang, X. Jia, and J. A. Benediktsson, "Probabilistic Fusion of Pixel-Level and Superpixel-Level Hyperspectral Image Classification," *IEEE Trans. Geosci. Remote Sens.*, vol. 54, no. 12, pp. 7416–7420, 2016, doi: 10.1109/TGRS.2016.2603190.
[11] C. M. Bishop, *Pattern Recognition and Machine Learning (Information Science and Statistics)*. Berlin, Heidelberg: Springer-Verlag, 2006.
[12] F. Wang, R. Zhang, and Q. Wu, "Hyperspectral image classification based on PCA network," *Work. Hyperspectral Image Signal Process. Evol. Remote Sens.*, vol. 0, pp. 1–5, 2016, doi: 10.1109/WHISPERS.2016.8071787.
[13] W. Burger and M. J. Burge, *Digital Image Processing*. in Texts in Computer Science. London: Springer London, 2016. doi: 10.1007/978-1-4471-6684-9.
[14] H. Liu, J. Sun, H. Sun, and H. Lin, "Image inpainting based on hidden Markov random field," in *2016 IEEE 13th International Conference on Signal Processing (ICSP)*, IEEE, Nov. 2016, pp. 697–701. doi: 10.1109/ICSP.2016.7877922.
[15] A. Blake, P. Kohli, and C. Rother, *Markov Random Fields for Vision and Image Processing*. The MIT Press, 2011. doi: 10.7551/mitpress/8579.001.0001.
[16] S. Kumar and R. L. Velusamy, "Kernel approach for similarity measure in latent fingerprint recognition," *International Conference on Emerging Trends in Electrical, Electronics and Sustainable Energy Systems, ICETEESES 2016*. pp. 368–373, 2016. doi: 10.1109/ICETEESES.2016.7581411.
[17] A. Yavariabdi and H. Kusetogullari, "Change Detection in Multispectral Landsat Images Using Multiobjective Evolutionary Algorithm," *IEEE Geosci. Remote Sens. Lett.*, vol. 14, no. 3, pp. 414–418, 2017, doi: 10.1109/LGRS.2016.2645742.
[18] I. Bakurov, M. Buzzelli, R. Schettini, M. Castelli, and L. Vanneschi, "Structural similarity index (SSIM) revisited: A data-driven approach," *Expert Syst. Appl.*, vol. 189, p. 116087, Mar. 2022, doi: 10.1016/j.eswa.2021.116087.
[19] X. Zhong *et al.*, "Fuzzy Nonlinear Proximal Support Vector Machine for Land Extraction Based on Remote Sensing Image," *PLoS One*, vol. 8, no. 7, p. e69434, Jul. 2013, doi: 10.1371/journal.pone.0069434.
[20] J. Huang, Y. Ma, X. Mei, and F. Fan, "A hybrid spatial-spectral denoising method for infrared hyperspectral images using 2DPCA," *Infrared Phys. Technol.*, vol. 79, pp. 68–73, Nov. 2016, doi: 10.1016/j.infrared.2016.09.009.
[21] C. A. Shah, "Automated lake shoreline mapping at subpixel accuracy," *IEEE Geosci. Remote Sens. Lett.*, vol. 8, no. 6, pp. 1125–1129, 2011, doi: 10.1109/LGRS.2011.2157951.